Heat Transfer Characteristic of Axisymmetric Under-expanded Impinging Jet on a Flat Surface

M. S. Yu, B. B. Kim**, H. H. Cho*, K. Y. Hwang*** and J. C. Bae****
*Yonsei University, **LG Cable Ltd, ***Agency for Defense Development
Yonsei University 134 Sinchon-dong, Seodaemun-gu, Seoul 120-749, Korea
hhcho@yonsei.ac.kr

Keywords: under-expanded impinging jet, shock wave, stagnation bubble, heat transfer coefficient

Abstract

An experimental study has been carried out to examine heat-transfer characteristics of an axisymmetric, under-expanded, sonic jet impinging on a flat plate and the local measurement of surface pressures and heat transfer coefficients on a plate have been achieved together with a visualization test of shock structure in a jet.

As a result, it has been found that the Nusselt number distribution has different aspects depending on the under-expansion ratios and the nozzle-to-plate distances.

Introduction

Various situations associated with the impingement of an under-expanded jet onto a solid object can be found in engineering applications. Among them, impingement of a jet engine exhaust, the take-off and landing of V/STOL aircraft, and the thrust vector control system of a solid rocket motor are some examples given frequently. Since dynamic energy is converted to thermal energy, impingement of high temperature flow like exhaust fumes may produce severe thermal loads as well as aerodynamic loads on the target surface. As results of extensive studies conducted by many researchers, some of the interesting and complex phenomena have been revealed to us, but not satisfactorily yet. A large portion related to this subject still remains unknown. A number of previous investigations associated with the under-expanded impinging jets have concentrated mainly on the basic aspects of flow structure: complex shock structures and interactions have been extensively studied using optical methods such as a shadowgraph and a Schlieren method[1-4], and the comparison with the theoretical predictions also have been performed.[5] Measurement of pressure distributions on the target surface has revealed an intriguing phenomenon of stagnation bubble which occurs around the stagnation point.[1-4] Since the 1990's, there have been several attempts to simulate numerically the flow field of supersonic impinging jet. In contrast to numerous investigations related to flow structures, very few data are available for heat transfer characteristics of the under-expanded impinging jets at present.

The objective of this study is to obtain basic heat transfer information on an under-expanded sonic jet which impinges on a flat plate. An investigation has been carried out to examine heat transfer characteristics of an axisymmetric under-expanded sonic jet. Distributions of heat transfer coefficient on the flat plate have been obtained in detail. In addition, distributions of surface pressure on the flat plate have been measured and the shock structures in the under-expanded jets have been visualized using a shadowgraph method. As the parameters of interest, the followings have been considered: one is the under-expansion ratio, which is defined by the ratio of the nozzle exit pressure to the ambient pressure. The other is the nozzle-to-plate distance. The emphasis is on the small nozzle-to-plate distances within the first shock cell. Finally, the effect of inclination of plate against the jet flow has been also considered in this study. The results of the present study would provide basic information to understand unknown aspects of heat transfer associated with under-expanded sonic jet impinging on a flat plate, and they might be used to verify the future numerical model related to sonic impinging jets.

Experimental Apparatus and Method

Experimental Apparatus

Figure 1 shows the schematic diagram of the experimental apparatus used for the present investigation. Air is compressed up to 150 kgf/cm^2 by a reciprocating compressor and passes through five stage air filters to remove moisture. Then, it is stored in 6 storage tanks. Total storage capacity of tanks is 690 liters. The compressed air is supplied to the settling chamber through regulators (Yamato sangyo, YR-5062) from the storage tanks. The nozzle, from which a jet issues, is mounted on the settling chamber. After stagnating at the settling chamber, the air is accelerated in the nozzle, and then injected into the atmosphere.

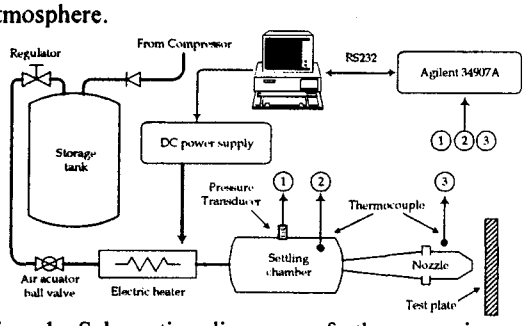

Fig. 1 Schematic diagram of the experimental apparatus.

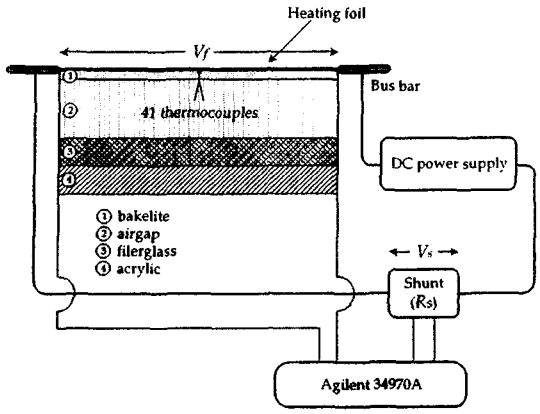

Fig. 2 Schematic diagram of the test plate for heat transfer measurement.

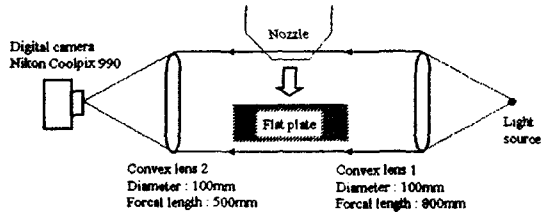

Fig. 3 Schematic diagram of the shadowgraph system.

The supplied air is heated with an electric heater positioned between storage tanks and settling chamber and the total temperature of a expanded jet is controlled to remain close to the ambient air temperature (within the difference of ±0.5K), to minimize the effect of entrainment of the ambient air with a different temperature.

The test plate for heat transfer measurement consists of the heating foil, the backing of insulated layers, and thermocouples. Figure 2 shows the schematic diagram of the test plate. Stainless steel heating foil is 25.4×10^{-3} mm thick, which is bonded on 3 mm thick bakelite plate with double-sided adhesive tape. The area of heated surface is 0.0354 m^2. When the electrical power is supplied, the heating foil provides constant heat flux condition. To determine the electrical power supplied to the surface, the voltage drop across the heating foil is measured during a run. The back side of the plate is insulated thermally with the air gap, fiberglass and acrylic. The plate is instrumented with a row of forty-one 36-gage T-type (copper-constantan) thermocouple junctions, and they are spaced 2.5 mm apart within 60 mm across the span in the central portion, where significant variation of temperature is expected, and 5 mm apart outside the center region.

Another plate with two pressure taps in the central portion is used for measurement of the surface pressure. The hole size is 0.8 mm diameter and the two pressure taps are spaced 20.0 mm. The pressure is measured by Druck pressure transducer (PMP4070) connected to each pressure tap. For getting the high data resolution, pressure taps are shifted with spacing of 1 mm and the voltage signals from pressure transducers are scanned three times and averaged.

The test plate is mounted on a linear motion system with two axes (Samik LMS, SAR1110T-200/400) driven by stepping motors (Oriental Motors, PK596NA). The stroke of the axial direction is 400 mm and that of the radial direction is 200 mm. The test plate can be traversed both in the axial direction and in the radial direction to an accuracy of 0.02 mm. Therefore, precise adjustment of nozzle-to-plate distance and the radial movement of pressure taps during the tests have been achieved.

The output signals from thermocouples and pressure transducers are scanned and acquired using Agilent 34970A data acquisition/switch units equipped with three HP 34902A 16-channel multiplexer modules and stored in a personal computer.

The flow field of a free jet is measured by a pitot pressure probe. The tip of the probe has outer diameter of 1.0 mm and inner diameter of 0.8 mm. The pitot probe is mounted on the traverse mechanism to scan the flow field during a test.

To visualize the shock structure in the flow field of the jet, shadowgraph method is used. Conventional shadowgraph system with a continuous light source of 30 W and two 100 mm diameter convex lenses is employed. The schematic diagram of the shadowgraph system is illustrated in Fig. 3. The parallel light is obtained by being passed through the convex lens, and it goes through the flow field near the nozzle exit. Optical image of flow field is photographed using a digital camera (Nikon, Coolpix 900) at a shutter speed of 1/500 of a second.

Experimental Procedure and Data Reduction

The experiments to obtain local heat transfer coefficients on the impinging plate are composed of two parts. First, the temperature distribution on the test plate is measured when the wall heat flux is zero, i.e., no electrical power is supplied to the heating foil on the surface. This provides adiabatic wall temperature distribution T_{aw}.

In the second part, under the same flow condition with the run for zero heat flux, the temperature distribution on the test plate is measured during the constant electric current is passing through the heating foil. Both temperature distributions are obtained by averaging the measured temperatures over 30 seconds after steady state is reached. In most cases, steady state is reached after about 4 minutes. Local heat flux, q_q is the averaged electrical power generated inside the heating foil. This heat flux is corrected for heat loss, q_l by conduction to the back of the test plate and radiation from the surface of heated foil.

$$q = q_q - q_l \tag{1}$$

$$q_q = \frac{IV_f}{A_f} = \frac{V_s}{R_s}\frac{V_f}{A_f} \tag{2}$$

where I is the electric current passing through heating foil and V_f, V_s, A_f are voltage drops across the

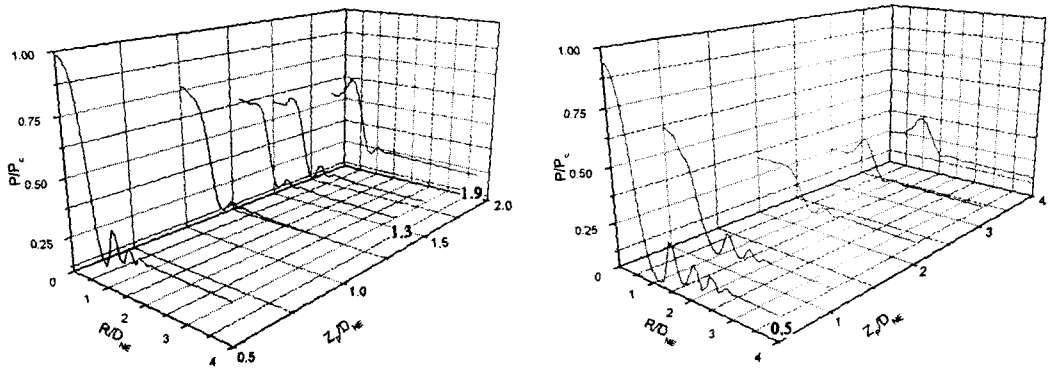

(a) P_e/P_a=2.0 (b) P_e/P_a=3.5

Fig. 4 Surface pressure profiles for different under-expansion ratios.

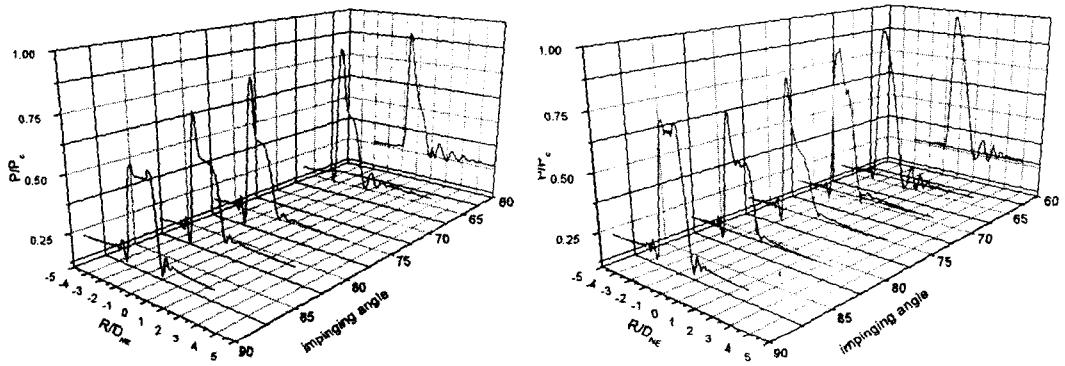

(a) Z_p/D_{ne}=1.5 (b) Z_p/D_{ne}=2.0

Fig. 5 Surface pressure profiles for various impinging angles.

heating foil and the shunt and the area of the heated surface respectively.

Finally, the local heat transfer coefficient is defined as a following simple equation and it is also presented in terms of the Nusselt number.

$$h = \frac{q}{T_w - T_{aw}} \tag{3}$$

$$Nu = \frac{hD_{NE}}{k_a} \tag{4}$$

As the experimental variables, the under-expansion ratio and the nozzle-to-plate are selected. The under-expansion ratio is defined as the ratio of nozzle exit pressure to the ambient pressure, i.e., P_e/P_a. During the experiment, P_e/P_a is varied from 1.5 to 3.5 including both of the moderate expanded and the highly expanded regions. The nozzle-to-plate distance is varied in the range from a half nozzle exit diameter to 20 diameters.

Results and Discussion

Surface Pressure and Visualized Shock Structure

The surface pressure on a stagnation point decreases initially with increasing nozzle-to-plate distance, and subsequent rise and fall repeat in the downstream direction.[6] For the sake of convenience, the nozzle-to-plate distance to which the central surface pressure decreases initially is referred to as initial expansion length, and it is denoted by Z_{ie}. Figure 4 shows surface pressure profiles within initial expansion length for different under-expansion ratios. In the case of P_e/P_a=2.0(Fig. 4(a)), when the plate is placed at Z_p/D_{NE}=0.5, the surface pressure profile has a maximum at the center of the plate, and the pressure drops as the flow accelerates with increasing radial distance from the stagnation point. The rapid fall of surface pressure near a stagnation region is due to the rapid flow acceleration rate in that region. Out of this region, surface pressure experiences a little fluctuations at the wall jet region and approaches to the ambient pressure (P_a/P_0=0.35). As the plate is moved downstream, the surface pressure in the shock

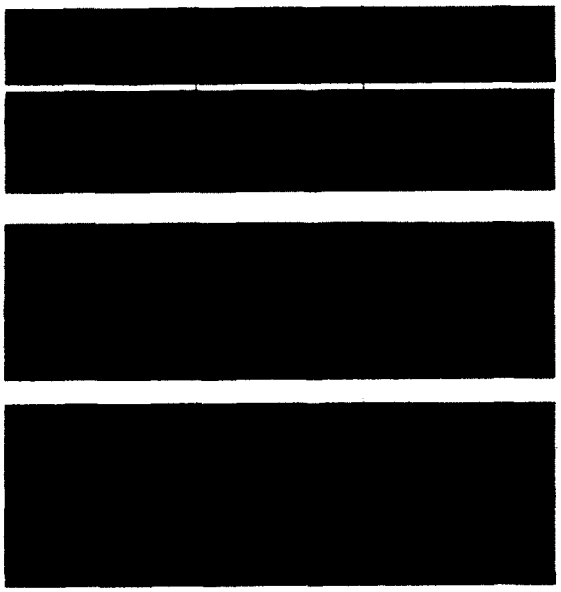

(a) P_e/P_a =2.0 (Z_p/D_{NE} =0.5, 0.75, 1.25 and 1.5)

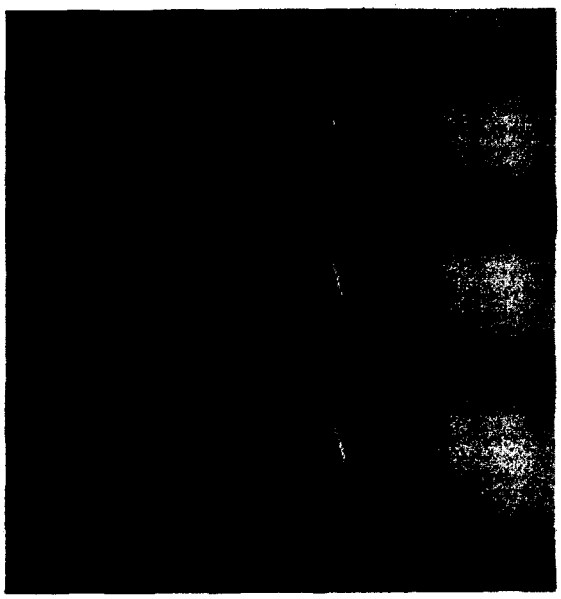

(b) P_e/P_a =3.5 (Z_p/D_{NE} =0.5, 1.0, 1.25 and 1.5)

Fig. 6 Shadowgraph results for shock structure in a jet

layer decreases because of the increased total pressure loss across the central stand-off shock with increasing upstream Mach number. As the plate is positioned further downstream(Z_p/D_{NE}=1.5 or 1.9), the maximum surface pressure appears at the annular region in the vicinity of the stagnation point. In according to the results suggested by other researchers[2], this peripheral maximum of the pressure appears due to the isolation of the re-circulating flow called a stagnation bubble in the central region.

Shadowgraph results for P_e/P_a =2.0 are presented in Fig. 6(a). At small nozzle-to-plate distances (Z_p/D_{NE}=0.5 or 0.75), the stand-off shock is almost flat over the span of the jet. Although the plate is moved away from the nozzle (Z_p/D_{NE}=1.25 or 1.5), the shock

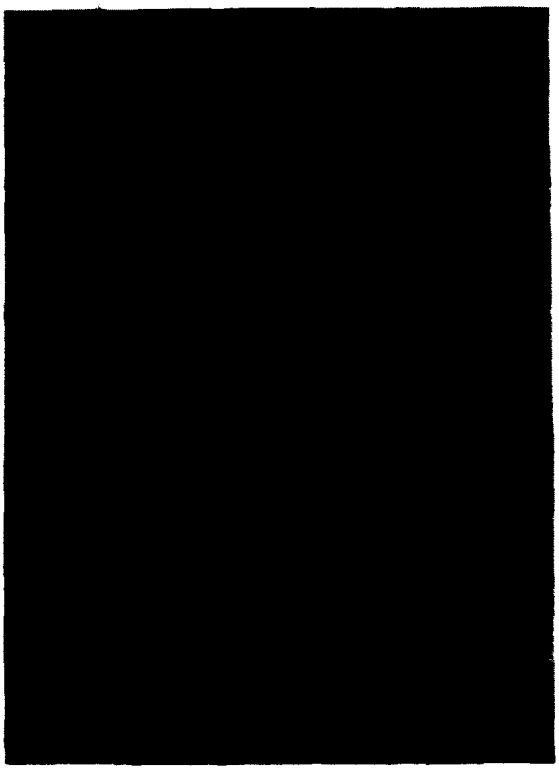

(c) Impinging angles of 90° , 75° and 60° respectively (P_e/P_a =2.0, Z_p/D_{NE} = 1.5)

Fig. 6 Shadowgraph results for shock structure in a jet

shape at the central part does not change while that at the outer region becomes oblique. Generally, the flow field between the stand-off shock and the impinging surface is divided into two regions: the inner flow which passes the flat central shock and the outer flow which passes the oblique shock. Due to the difference of shock intensity, the total pressure of the inner flow is less than that of outer flow. Mixing zone is developed along the slip-line while exists between the two flows, and the interaction of this high-pressure shear layer with the boundary layer causes separation, which results in the appearance of a peripheral static pressure maximum and the formation of the stagnation bubble.[3]

Even when the under-expansion ratio increases to 3.5, the radial profiles of surface pressure in the shock layer have similar variation with increasing nozzle-to-plate distance. And the pressure fluctuation in a wall jet region also appears obviously at the nozzle-to-plate distances of Z_p/D_{NE}=0.5, 1.0 in Fig. 4(b). This phenomenon in the wall jet region is occurred by the repeated reflections of the waves from the jet edge by the upper boundary of the wall jet and the plate surface.[4]

As the plate is moved downstream of initial expansion length, total pressure in the central region is recovered due to the inward diffusion from outer region behind the oblique shock. The pressure recovery occurs steeply in the case of P_e/P_a=2.0

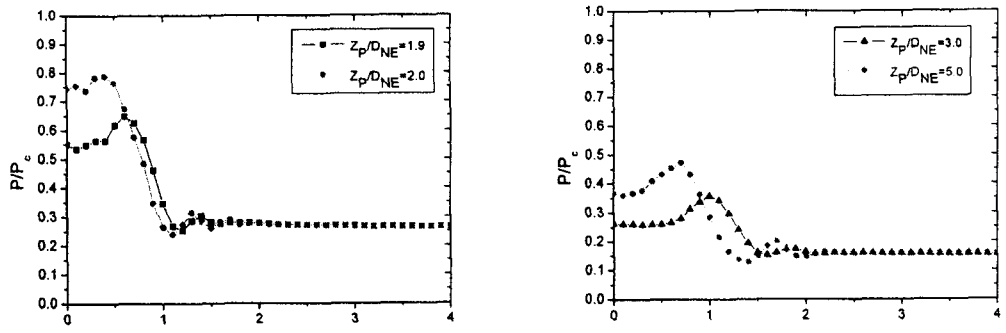

(a) P_e/P_a=2.0 (b) P_e/P_a=3.5

Fig. 7 Pressure recovery downstream of the initial expansion length.

because the central stand-off shock diminishes significantly in size. However, for higher P_e/P_a, pressure recovery occurs very slowly even if the surface is moved downstream of the initial expansion length. It is due to the inward diffusion is less effective due to the existence of subsonic core behind of the central shock. These pressure recovery phenomena can be seen in Fig. 7.

Figure 5 shows the surface pressure profiles when the impinging surface is inclined against the jet flow. In this case, the under-expansion ratio is fixed to P_e/P_a=2.0 and the nozzle-to-plate distance is considered to Z_p/D_{NE}=1.5 and 2.0. Impinging angle is changed from 60° to 90°. In this study, impinging angle is 90° when the plate is perpendicular to the jet flow and it becomes small if rotation angle of plate increases. In the figure, the negative R direction is referred to as 'upward' and the positive R direction is referred to as 'downward'. In Fig. 5, the position where the maximum pressure appears moves slightly upward as the impinging angle decreases. Also, the magnitude of maximum pressure value increases with decreasing impinging angle and it is $0.9P_c$ at Z_p/D_{NE}=1.5 and $0.97P_c$ at Z_p/D_{NE}=2.0 for the impinging angle of 60°. This phenomenon occurs due to the movement of the stagnation streamline into the upper tail shock region for inclined jet impingement.[7] The upward pressure decreases abruptly to the level of the ambient pressure because the expansion fans are formed at the intersection of the tail shock and the jet edge. The shadowgraph results of impinging jets at various impinging angles can be seen in Fig. 6(c) for the nozzle-to-plate distance of Z_p/D_{NE}=1.5.

Heat Transfer Coefficient

Figure 8 and 9 show the radial profiles of Nusselt number on the impinging surface for different under-expansion ratios. The profiles have very complex variations depending on the nozzle-to-plate distance.

For the under-expansion ratio of 2.0(Fig.8), immediately downstream of the nozzle exit, Nusselt number has a central peak at the stagnation point and an annular peak at $R/D_{NE}\approx\pm2$. From the pressure distribution at the same position (Fig. 4(a)), marked pressure variations are not observed where the annular peak of Nusselt number appears. From the explanations given by previous investigators[5,7,8], the appearance of the annular peaks seems to be related to the increased turbulence, whether it results from transitions of boundary layer or growth of vortex rings in the upper boundary in the wall jet region.

When the plate is positioned to Z_p/D_{NE}=1.0 or 1.25, another annular peak appear near the stagnation point. This phenomenon can be explained as follows. When the plate is located near the initial expansion length, the mixing zone developed along the slip line affects the inner region near the stagnation point resulting in the high turbulence level and also the enhancement of the heat transfer.

As the plate is moved further downstream, the annular peak moves inward and gradually disappears. Beyond Z_p/D_{NE}=10.0, the radial variation of Nusselt number has a simple bell shape and the Nusselt number has a maximum at the stagnation point and declines smoothly in the radial direction. At these positions, jet flow in the central region becomes the turbulence flow due to the shear or mixing with the outer flow, so the Nusselt number has a maximum value at the stagnation point.

When the under-expansion ratio increases to 3.5 (Fig.9), general trends in variation with nozzle-to-plate distance are similar to those for P_e/P_a=2.0 but the core region with low Nusselt number maintains to the longer nozzle-to-plate distances due to the larger size of stand-off shock and subsonic flow with small momentum behind it. In the figure, the inner peak starts to appear at Z_p/D_{NE}=1.5 and disappears at Z_p/D_{NE}=10.0.

Figure 10 shows the radial profiles of Nusselt number on the impinging surface for various impinging angles. In the same manner with pressure measurement test, the under-expansion ratio is set to 2.0 and the nozzle-to-plate distances of Z_p/D_{NE}=1.5 and 2.0 are considered. As seen in Fig. 10(a), Nusselt

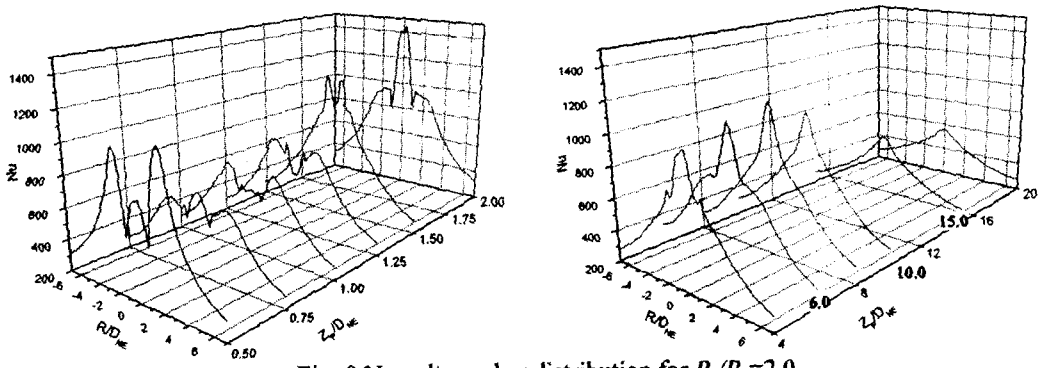

Fig. 8 Nusselt number distribution for P_e/P_a=2.0.

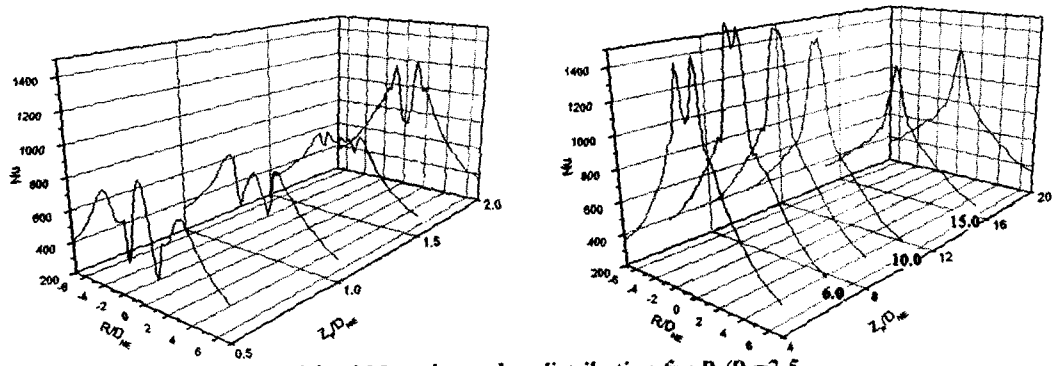

Fig. 9 Nusselt number distribution for P_e/P_a=3.5.

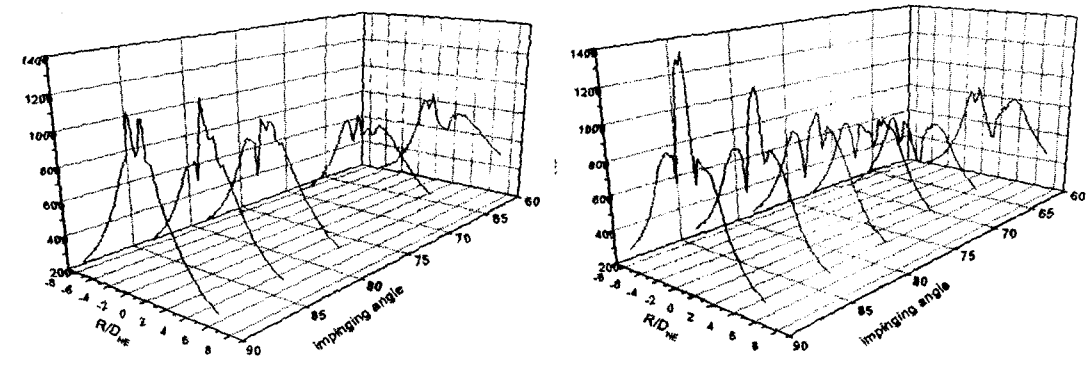

(a) Z_p/D_{ne}=1.5 (b) Z_p/D_{ne}=2.0

Fig. 10 Nusselt number distribution for P_e/P_a=2.0 for various impinging angles.

number in the central region decreases significantly as the impinging angle decreases at Z_p/D_{NE}=1.5. Two peaks occur near $R/D_{NE}\approx\pm0.5$ for perpendicular impingement, and both of the peak values decrease with decreasing impinging angle. While the decrease in the upward peak value ceases at the impinging angles less than 70°, the downward peak near $R/D_{NE}\approx+0.5$ continues to decrease and disappears at the impinging angle of 60°. In the wall jet region, Nusselt number in the upward direction decreases with decreasing impinging angle, but such a tendency is reversed in the downward region.

Nomenclature

T_{aw}	: adiabatic wall temperature
q_q	: averaged electrical power from the heating foil
q_l	: heat loss by conduction to the backside of impinging plate
V_f	: voltage drops across the heating foil
V_s	: voltage drops across the shunt
A_f	: area of the heated surface
D_{NE}	: diameter of nozzle exit
P	: surface pressure on the impinging surface
P_e	: static pressure at nozzle exit

P_a : ambient pressure
P_c : pressure in the settling chamber
Z_{ie} : initial expansion length
Z_P : distance in axial direction between the plate and nozzle exit
R : distance in radial direction from the center point of impinging plate

Conclusion

An experimental investigation has been conducted to examine heat transfer characteristics of an axisymmetric, under-expanded jet impinging on a flat plate. Depending on the under-expansion ratios, nozzle-to-plate distances and the impinging angles, the Nusselt number distribution has different aspects. Annular peak, which appears at small nozzle-to-plate distances is related to the increased turbulence by transition of boundary layer or growth of vortex rings in the wall jet region. When the mixing layer developed along the slip line affects the inner region near the stagnation point, another peak of Nusselt number appears inside of annular peak. According to increasing nozzle-to-plate distance, heat transfer coefficient at central region increases due to encroachment of mixing layer into the center of the jet. When the impinging angle decreases, overall values of Nusselt number decreases at the central region and the annular peak maintains at the upward region better than at the downward region. At the wall jet region, heat transfer increases at the downward region with decreasing impinging angle and the tendency is reversed at the upward region.

Acknowledgement

This research was supported by Agency for Defense Development and by Ministry of Science & Technology through their National Research Laboratory program.

References

1) Gubanova, O. I., Lucev, V. G., and Plastina, L. N.: Central Breakaway Zone with Interaction between a Supersonic Underexpanded Jet and a Barrier, Fluid Dynamics, Vol. 6, 1973, pp.298-301.
2) Kalghatgi, G. T., and Hunt, B. L.: The Occurrence of Stagnation Bubbles in Supersonic Impingement Flows, The Aeronautical Quarterly, Vol. 27, No. 3, 1976, pp. 169-185.
3) Ginzburg, I. P., Semiletenko, B. G., Terpigorev, V. S., and Uskov, V. N.: Some Singularities of Supersonic Underexpanded Jet Interaction with a Plane Obstacle, Journal of Engineering Physics, Vol. 19, 1973, pp. 1081-184.
4) Carling, J. C., and Hunt, B. L.: The Near Wall Jet of a Normally Impinging, Uniform, Axisymmetric, Supersonic Jet, Journal of Fluid Mechanics, Vol. 66, Part 1, 1974, pp. 159-176.
5) Gardon, R., and Akfirat, J. C.: The Role of Turbulence in Determining the Heat Transfer Characteristics of Impinging Jets, International Journal of Heat and Mass Transfer, Vol. 8, 1965, pp. 1261-1272.
6) Kim, B. G., Yu, M. S., and Cho, H. H.: Recovery Temperature Measurement of Under-expanded Sonic Jets Impinging on a Flat Plate, Journal of Thermophysics and Heat Transfer, Vol. 17, No. 3, 2003, pp. 313-319.
7) Lamont, P. J., and Hunt, B. L.: The Impingement of Underexpanded, Axisymmetric Jets on Perpendicular and Inclined Flat Plates, Journal of Fluid Mechanics, Vol. 100, Part 3, 1980, pp. 471-511.
8) Gardon, R. and Cobonpue, J.: Heat Transfer between a Flat Plate and Jets of Air Impinging on It, International Developments in Heat Transfer, 1962, pp. 454-460.
9) Goldstein, R. J., Behbahani, A. L., and Heppelmann, K. K.: Streamwise Distribution of the Recovery Factor and the Local Heat Transfer Coefficient to an Impinging Circular Air Jet, International Journal of Heat and Mass Transfer, Vol. 29, 1986, pp. 1227-1235.